Theor Chem Acc (2012) 131:1266
DOI 10.1007/s00214-012-1266-z

REGULAR ARTICLE

Theoretical studies of COOH group effect on the performance of rhenium (I) tricarbonyl complexes with bispyridine sulfur-rich core ligand as dyes in DSSC

Ting-Ting Zhang · Jianfeng Jia · Hai-Shun Wu

Received: 28 March 2012 / Accepted: 13 August 2012 / Published online: 30 August 2012

Abstract The series of rhenium (I) tricarbonyl mixed-ligand complexes $ReCl(CO)_3(H_nbpydt)$ ($n = 2$, **1**; $n = 4$, **2**; bpy = bispyridine, d*t* = 1,3-dithiole) and $ReCl(CO)_3(H_nbpyTTF)$ ($n = 2$, **3**; $n = 3$, **4**; TTF = Tetrathiafulvalene) have been investigated theoretically to explore the effect of COOH functional group on their electronic structures, spectroscopic properties and their properties as dye in a solar cell. The calculated geometry structure and absorption spectrum of **1** and **3** are generally consistent with the experimental results. By attaching the COOH groups on both bpy and d*t* (TTF in **4**) moiety in **2**, the nature of LUMO is also contributed by both π^*(bpy) and π^*(d*t*) (π^*(TTF) in **4**), and the absorptions have an obvious red shift compared with **1** and **3**. In addition, it can be found that the transition terminates at the orbital populated by the COOH-appended moieties, and the performance of **2** and **4** in the dye-sensitized solar cell can be enhanced as compared with **1** and **3**.

Keywords Rhenium (I) complexes · Electronic structure · Spectroscopic property · Time-dependent density functional theory

1 Introduction

Considerable efforts have been devoted to research the dye-sensitized solar cells (DSSCs) for the conversion of sunlight into electricity because of their low cost and high efficiency [1–4], which has recently reached 12 % energy efficiency [5]. The operation of DSSCs has been reviewed elsewhere [6–8]. Further increases in efficiency can come in a number of areas, one of which is improving the property of the dye sensitizer. The dye sensitizer is one of the key components of DSSCs for achieving high power conversion efficiency, which is used to sensitize the semiconductor electrode. To date, the most efficient and stable dye molecules for this application have been Ru(II) polypyridyl complexes [9–12]. For example, Ru(II) polypyridyl complexes with carboxylate, [Ru(bpp)(dcbpyH_2)Cl] + (bpp = 2,6-bis(*N*-pyrazolyl)pyridine, dcbpyH_2 = 2,2′-bipyridine-4,4′-dicarboxylic acid) [3] have been synthesized and analyzed, in which the carboxylic acid pendants are key to the attachment of dyes to the semiconductor surface [13].

Similar to ruthenium compounds, tricarbonyl rhenium(I) polypyridine complexes with carboxylic pendants are attractive research targets owing to their photophysical, photochemical, excited-state redox properties and potential role as a dye for DSSC application [14–17]. More important for this study is the fact that the Re(II/I) reduction potentials are significantly 0.5–1 eV positive of those from other inorganic sensitizers. In principle, this provides a larger driving force for donor oxidation and interfacial charge recombination. In addition, the facial geometry about Re(I) likely affords more uniform molecular orientation on TiO_2 than does the commonly utilized *cis*-$Ru(dcb)_2(NCS)_2$ sensitizer [18]. The Re(I) coordination compounds, *fac*-Re(deeb)$(CO)_3$(X), (deeb = 4,4′-(COOEt)$_2$-2,2′-bipyridine, X = I^-, Br^-, Cl^-, or CN^-), and [*fac*-Re(deeb)$(CO)_3$(py)](OTf), (OTf^- = triflate, py = pyridine), have been prepared and anchored to nanocrystalline (anatase) TiO_2 [19].

Electronic supplementary material The online version of this article (doi:10.1007/s00214-012-1266-z) contains supplementary material, which is available to authorized users.

T.-T. Zhang · J. Jia · H.-S. Wu (✉)
School of Chemistry and Materials Science,
Shanxi Normal University, Linfen 041004, China
e-mail: wuhssxtu@163.com

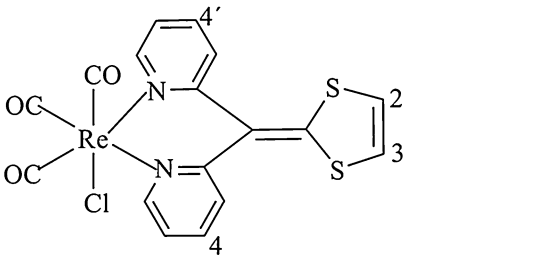

1 2, 3 in dt = COOH
2 2, 3 in dt; 4,4′ in bpy = COOH

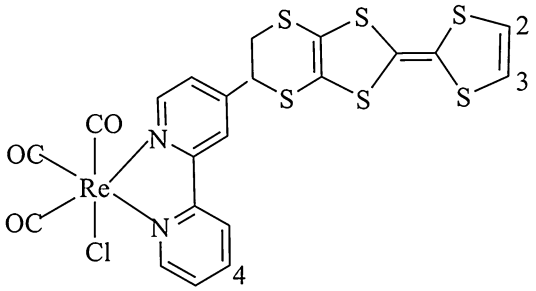

3 2, 3 in TTF = COOH
4 2, 3 in TTF; 4 in bpy = COOH

Fig. 1 Schematic representation of **1**–**4**

Recently, a series of Re(I) tricarbonyl bispyridine complexes containing sulfur-rich core ligand and free carboxylic acid pendants, $ReCl(CO)_3(H_2bpydt)$ and $ReCl(CO)_3(H_2bpyTTF)$ (d*t* = 1,3-dithiole, TTF = Tetrathiafulvalene, bpy = bispyridine), have been synthesized, and the photovoltaic performance as photosensitizers in the nanocrystalline TiO_2-based solar cells was studied [20]. The d*t* and TTF ligands incorporating bpy have received much attention for decades, on account of their highly desirable properties and growing utility as versatile building blocks in molecular, supramolecular and materials chemistry [21–24]. From the experimental point of view, the study about Re(I) tricarbonyl complexes containing multi-sulfur ligands as photosensitizers is poor. The sulfur atoms in a dye structure can have significant effects on the overall DSSC cell performance [25–27]. In addition, we think the performance of the new Re(I) complexes as photosensitizers can be improved by adjusting the number and position of COOH group on the ring system. Therefore, a deep insight into the structures and photovoltaic properties for this kind of complexes is much needed and significant.

Indeed, computational studies can help us in realizing the assumption and providing some hints about some important aspects of the studies dyes. The excellent agreement of calculated results with available experimental data indicates that the approach could be used as an efficient predictive tool to research the new photosensitizer [28–30]. For example, De Angelis firstly addressed the problem of metalorganic dye energetics from a computational point of view [31].

Thus in this paper, we take $ReCl(CO)_3(H_2bpydt)$ (**1**) and $ReCl(CO)_3(H_2bpyTTF)$ (**3**) as parent models, and theoretical calculations were employed to reform the system by adjusting the number of COOH group and their attaching point on ppy ligand (four COOH groups in **2** and three COOH groups in **4**, see Fig. 1) in order to enhance the performance of the dyes. In addition, the electronic structures, absorption spectrum, as well as the redox potentials of the systems, were calculated to further understand the mechanism as dyes and explore the performance as dyes. The results will broaden the field of studies on synthesizing and designing new dyes.

2 Computation methods

All of the calculations were accomplished with the Gaussian 03 software package [32]. A hybrid Hartree–Fock/density functional theory (HF/DFT) model approach based on the Perdew-Burke-Erzenrhof (PBE) functional [33, 34], referred to as PBE1PBE, where the HF/DFT exchange ratio is fixed a priori to 1/4, was used to optimize the ground state. There were no symmetry constraints on these complexes. In the calculations, the quasi-relativistic pseudo-potentials of Re atoms proposed by Hay and Wadt [35, 36] with 14 valence electrons were used, and a "double-ξ" quality basis set LANL2DZ associated with the pseudo-potential was adopted. A relativistic effective core potential (ECP) on Re replaces the inner core electrons leaving the outer core $[(5s^2)(5p^6)]$ electrons and the $(5d^6)$ valence electrons for Re(I). The 6-31G(d) basis bet was adopted for the no-metal atoms.

On the basis of the optimized geometry structures in the ground states, the molecular orbital compositions and the vertical transition energies to the valence excited states in methanol media were calculated by time-dependent density functional theory (TD-DFT) [37–39] at the PBE1PBE hybrid functional level with the same basis set. The optimized ground state geometry was studied in methanol as an approximation to include solvent polarization effects, and the polarized continuum model (PCM) [40, 41] was adopted to simulate the solvent field of methanol in TD-DFT calculation. The rationality of approximate calculation has been proven to be reliable in recent studies [42–46] and gave good agreement with experimental spectra.

The standard redox potentials of the complexes $[ReCl(CO)_3L]$ in the ground state, E^0, relative to the standard calomel electrode (SCE) can be calculated using Eq. (1) on the basis of the thermodynamic cycle [46] as shown in Fig. S1 (Supplementary Materials).

$$E^0_{[\mathrm{ReCl(CO)_3L}]^+/[\mathrm{ReCl(CO)_3L}]} = -\frac{\Delta G^0_{[\mathrm{ReCl(CO)_3L}]^+/[\mathrm{ReCl(CO)_3L}]} - \Delta G^0_{\mathrm{SCE}}}{nF} \quad (1)$$

where,

$$E^0_{[\mathrm{ReCl(CO)_3L}]^+/[\mathrm{ReCl(CO)_3L}]} = -\Delta G^0_{\mathrm{aq}} \quad (2)$$

$$\Delta G^0_{\mathrm{aq}} = \Delta G^0_{\mathrm{gas}} + \Delta G^0(2) - \Delta G^0(1) \quad (3)$$

$$\Delta G^0(1) = G^0[\mathrm{ReCl(CO)_3L}](\mathrm{aq}) - G^0[\mathrm{ReCl(CO)_3L}](\mathrm{gas}) \quad (4)$$

$$\Delta G^0(2) = G^0[\mathrm{ReCl(CO)_3L}]^+(\mathrm{aq}) - G^0[\mathrm{ReCl(CO)_3L}]^+(\mathrm{gas}) \quad (5)$$

$\Delta G^0_{\mathrm{SCE}} = -4.1888\,\mathrm{eV}$ [47], $F = 23.06\,\mathrm{kcal\,mol^{-1}\,V^{-1}}$. All of the related free energies were calculated under standard conditions, that is, at 298.15 K and 1 atm.

3 Results and discussion

3.1 Geometry structures in the ground state

The optimized structures of **1–4** are shown in Fig. 2, and the main geometry parameters are summarized in Table 1 in comparison with the available experimental values [20] of $ReCl(CO)_3$(Medpydt) and $ReCl(CO)_3$(MebpyTTF), the hydrolysis product of which is complexes **1** and **3**, respectively. They are very similar in the structure. Vibrational frequencies were calculated on the basis of the optimized geometries of **1–4** to verify that each of the geometries is a minimum on the potential energy surface.

The optimized bond lengths and bond angles are in general agreement with the corresponding experimental values from Table 1. All the structures show the Re(I) adopts a distorted octahedral coordination geometry, with the chemically robust *fac*-$[Re(CO)_3]^+$ core and the halide is slightly tilted toward the N^N unit. The bond lengths of Re–C and Re–Cl are consistent with those found in similar tricarbonyl Re(I) complexes [48] and N(1)–Re–N(2) angle are characteristically smaller than the ideal value of 90°, imposed by the rigid geometry of the chelating bipyridine (bpy) ligands. In complex **1**, the two aromatic rings form a "butterfly-like" substructure due to the flexibility of the bpy moiety [20] and the Re–N distances are almost identical, which are in general agreement with the relatively symmetrical structure of ligand Medpydt. In complex **3**, the π conjugation within the TTF unit is extended to all six sulfur atoms, but the C(4)–C(5) bond is significantly longer than the C(6)–C(7) bond, which revealing the single-bond nature of C(4)–C(5) bond, and this precludes the π conjugation between the bpy and TTF unit. According to calculations, the bpy unit was substituted by –COOH group in **2** and **4**, but they have similar geometrical rearrangements to **1** and **3** respectively.

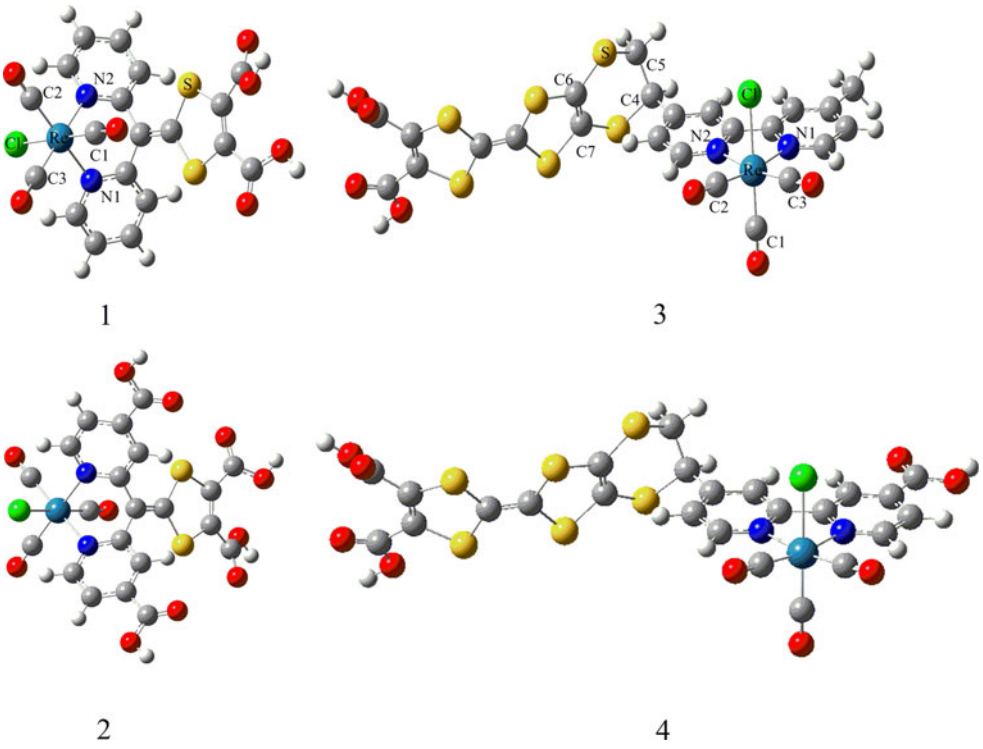

Fig. 2 Ground-state structures of **1–4** optimized by PBE1PBE

Table 1 The optimized main geometry parameters for **1–4** in ground state, together with the experimental values

	1		**2**	**3**		**4**
	S_0	exptl[a]	S_0	S_0	exptl[b]	S_0
Bond length (Å)						
Re–N(1)	2.207	2.206	2.200	2.173	2.165	2.165
Re–N(2)	2.208	2.207	2.201	2.173	2.152	2.172
Re–C(1)	1.904	1.857	1.906	1.909	1.897	1.911
Re–C(2)	1.915	1.879	1.917	1.918	1.928	1.921
Re–C(3)	1.915	1.889	1.917	1.917	1.860	1.918
Re–Cl	2.485	2.473	2.483	2.484	2.482	2.482
C(4)–C(5)				1.537	1.438	1.537
C(6)–C(7)				1.348	1.315	1.348
Bond angle (deg)						
N(1)–Re–N(2)	81.5	83.2	81.7	74.6	75.0	74.9
N(1)–Re–C(2)	173.8	174.0	174.4	170.7	175.1	170.7
N(2)–Re–C(3)	173.6	177.9	174.3	170.5	173.5	170.6
Cl–Re–C(1)	177.0	175.6	177.1	175.9	175.7	176.3

[a, b] Experimental data from Ref. [16]

3.2 Frontier molecular orbital properties

The partial frontier molecular orbital (FMO) compositions and energy levels of **1–4** are listed in Tables S1–4 (Supplementary Materials), respectively. It will be useful to examine the FMOs of these Re complexes to provide the framework on the excited state.

The calculated results showed that lowest unoccupied molecular orbital (LUMO) of **1** is mostly concentrated on the d*t* group, while the LUMO + 1 is localized on both bpy and d*t* ligands. The highest occupied molecular orbital (HOMO) is composed of d(Re), π(bpy), and π(d*t*), while other higher occupied molecular orbitals have strong d(Re) (>42 %) mixed with π(Cl) and π(CO) characters. When the COOH groups are anchored to both d*t* and bpy in **2**, the LUMO is contributed by π^*(bpy) and π^*(d*t*) and the LUMO + 1 is predominantly of π^*(d*t*). The HOMOs for **2** have the similar composition to **1**. Compared **4** with **3**, analogously, the contribution of LUMO is changed from π^*(bpy) to π^*(bpy) and π^*(TTF), while the LUMO + 1 is changed from π^*(TTF) to π^*(bpy) and π^*(TTF). The HOMOs of **3** and **4** lie primarily on the π(TTF) (>95 %), while other occupied molecular orbitals are substantially mixed with the d(Re) character. Moreover, the COOH groups attached to bpy moiety in **2** and **4** can decrease the energy levels of the LUMO more significantly than those of the HOMO and thus sufficiently stabilize the LUMO, resulting in narrower HOMO–LUMO energy gaps.

From the above analysis, the FMOs are influenced by the number and position of COOH group. Particularly, the LUMOs are mainly mastered by the ligands attached by the COOH groups. This is an important feature for the complex to act as the dyes in DSSC. Since the complex can interact with the semi-conductor via the COOH group, the transferred electron can reach the conduction band of the semiconductor via the virtual orbitals attached by COOH groups [49]. This is vital for a larger charge collection efficiency.

3.3 Absorptions in methanol media

The calculated absorption energies associated with their oscillator strengths, the main configurations, and their assignments, as well as the experimental results of **1** and **3**, are given in Table 2. The fitted absorption curves of **1–4** are shown in Fig. 3. Figure 4 displays the energy levels of molecular orbital involved in the lowest-lying absorption transitions of **1–4**, which can intuitively understand the transition process. The experimental and calculated absorptions are compared in Figs. 5 and 6 for **1** and **3**, respectively.

Figure 4 and Table 2 show the lowest-lying singlet → singlet absorption band of **1** is at 2.89 eV (429 nm) and the excitation configuration of HOMO → LUMO is responsible for the transition. As shown in Table S1, this excitation can be assigned to{[d(Re) + π(bpy) + π(d*t*)] → [π^*(d*t*)]}transition with mixing $ML_{dt}CT/L_{bpy}L_{dt}CT/IL_{dt}CT$ (metal-to-ligand charge transfer/ligand-to-ligand charge transfer/intra-ligand charge transfer) transition character, and the COOH groups take part in the transition process. However, it cannot be differentiated in the measured spectrum, this may be due to its weak oscillator strength (0.0485, the weakest among the calculate absorptions). For the other two strong absorptions at 378

Table 2 Selected calculated excitation energies (E, eV), wavelengths (λ, nm), oscillator strengths (f), driving force of charge injection (D, in V), and dominant excitation character of **1**–**4**, together with the available experimental absorption data of **1** and **3** (ε, 10^3 M^{-1} cm^{-1})

Transition	|CI| (coeff.)	E	D	λ_{cal}	λ_{exp} (ε)[a]	f	Character
1							
H → L	0.69436 (96 %)	2.89	0.65	429		0.0485	$ML_{dt}CT/L_{bpy}L_{dt}CT/IL_{dt}CT$
H → L + 1	0.69151 (96 %)	3.28	1.06	378	401 (8.7)	0.1706	$M(L_{bpy}L_{dt})CT/I(L_{bpy}L_{dt})CT$
H → L + 3	0.60924 (74 %)	3.92	1.68	316	323 (6.1)	0.0851	$M(L_{bpy}L_{dt})CT/I(L_{bpy}L_{dt})CT$
H − 1 → L + 6	0.31727 (20 %)	5.17	2.93	240		0.0704	$ML_{dt}CT/L_{Cl}L_{dt}CT/L_{CO}L_{dt}CT$
H − 3 → L + 7	0.29960 (18 %)						$ML_{CO}CT/ML_{bpy}CT/IL_{CO}CT/L_{CO}L_{bpy}CT$
2							
H → L	0.69968 (98 %)	2.76	0.48	449		0.0951	$M(L_{bpy}L_{dt})CT/I(L_{bpy}L_{dt})CT$
H → L + 1	0.66833 (89 %)	2.98	0.70	416		0.0442	$M(L_{bpy}L_{dt})CT/I(L_{bpy}L_{dt})CT$
H → L + 3	0.69933 (98 %)	3.73	1.45	333		0.1524	$M(L_{bpy}L_{dt})CT/I(L_{bpy}L_{dt})CT$
H − 1 → L + 4	0.38761 (30 %)	4.62	2.34	269		0.0558	$ML_{bpy}CT/L_{Cl}L_{bpy}CT/L_{CO}L_{bpy}CT$
H → L + 5	0.32564 (21 %)						$M(L_{bpy}L_{dt})CT/I(L_{bpy}L_{dt})CT$
H → L + 6	0.30459 (19 %)						$ML_{CO}CT/ML_{dt}CT/(L_{bpy}L_{dt})L_{CO}CT/IL_{dt}CT$
H − 1 → L + 7	0.42819 (37 %)	4.89	2.61	254		0.0494	$ML_{CO}CT/ML_{bpy}CT/L_{Cl}L_{CO}CT/L_{Cl}L_{bpy}CT/IL_{CO}CT$
H − 1 → L + 4	0.34610 (24 %)						$M(L_{bpy}L_{dt})CT/I(L_{bpy}L_{dt})CT$
3							
H → L + 1	0.69134 (96 %)	2.39	1.06	520		0.0240	$IL_{TTF}CT$
H − 3 → L	0.59215 (70 %)	3.19	1.86	389	398 (5.4)	0.0952	$ML_{bpy}CT/L_{Cl}L_{bpy}CT/L_{CO}L_{bpy}CT/L_{TTF}L_{bpy}CT$
H − 2 → L	0.35799 (26 %)						$ML_{bpy}CT/L_{TTF}L_{bpy}CT$
H → L + 7	0.51374 (53 %)	4.22	2.89	294	298 (29.3)	0.6550	$IL_{TTF}CT$
H − 5 → L	0.21886 (10 %)						$L_{TTF}L_{bpy}CT/IL_{bpy}CT$
4							
H → L	0.69907 (98 %)	2.22	0.75	559		0.0080	$L_{TTF}L_{bpy}CT/IL_{TTF}CT$
H − 3 → L	0.64262 (83 %)	2.92	1.45	424		0.0944	$M(L_{bpy}L_{TTF})CT/L_{Cl}(L_{bpy}L_{TTF})CT/L_{CO}(L_{bpy}L_{TTF})CT$
H → L + 7	0.39122 (31 %)	4.21	2.74	294		0.3481	$IL_{TTF}CT$
H − 3 → L + 3	0.29425 (17 %)						$M(L_{bpy}L_{TTF})CT/L_{Cl}(L_{bpy}L_{TTF})CT/L_{CO}(L_{bpy}L_{TTF})CT$
H − 1 → L + 3	0.26855 (14 %)						$M(L_{bpy}L_{TTF})CT/L_{TTF}L_{bpy}CT/IL_{TTF}CT$

[a] The experimental absorption data are from Ref. [20]

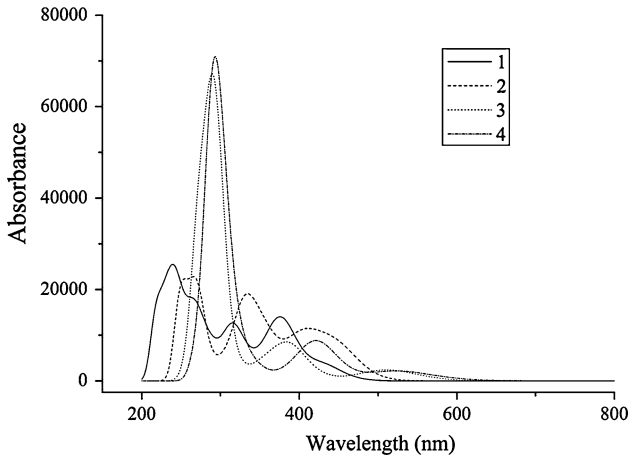

Fig. 3 Simulated absorption spectra of **1**–**4** in methanol

and 316 nm, the excitations responsible for them originate from the same occupied orbital (HOMO) but terminate in the different virtual orbital, but they have the same transition character $M(L_{bpy}L_{dt})CT/I(L_{bpy}L_{dt})CT$. In addition, the absorptions are comparable to the measured values at 401 and 323 nm, respectively. Thus, a very good agreement with the experimental spectrum is obtained when the PBE1PBE hybrid functional is used together with the PCM model for methanol solvent. The strongest absorption at 240 nm is contributed by excitations H − 1 → L + 6 and H − 3 → L + 7 with mixed transition characters.

The absorption of **2** is similar to that of **1** in profile but with obvious red shift (Fig. 3), which is consistent with the variation rules of the HOMO–LUMO energies gaps. Furthermore, different from the lowest-lying absorption band of **1**, the transition terminates in both bpy and d*t* moieties, which are subligated by the COOH groups. Therefore, the lowest energy absorption of **2** at 449 nm can be attributed to {[d(Re) + π(bpy) + π(d*t*)] → [π* (bpy) + π*(d*t*)]} transition with the $M(L_{bpy}L_{dt})CT/I(L_{bpy}L_{dt})CT$ transition character. The other higher absorption spectra of **2** are

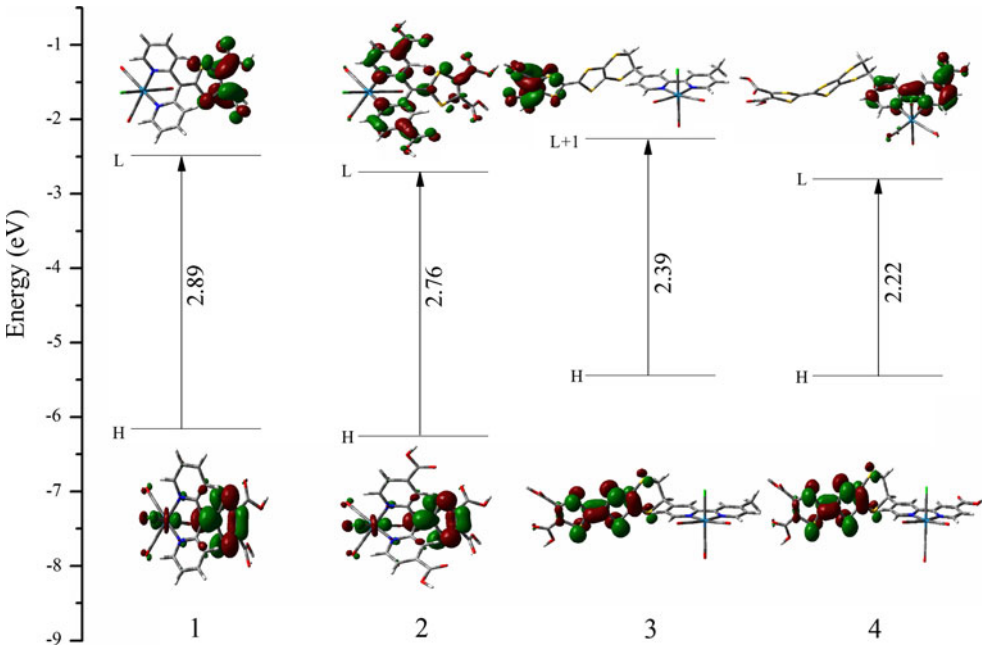

Fig. 4 Transitions responsible for the lowest-lying absorptions for **1**–**4**

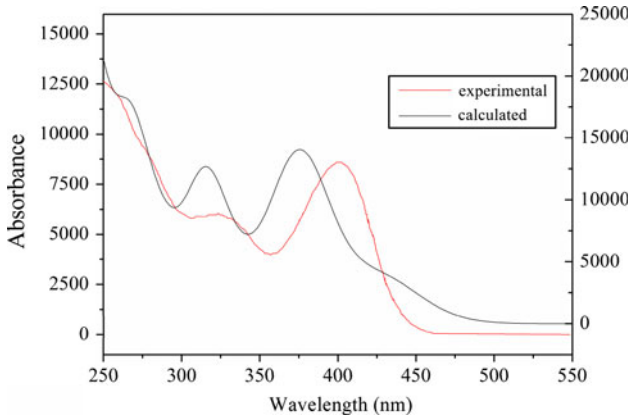

Fig. 5 The experimental and calculated absorption spectra of **1** (*red line* experimental spectrum [20], linked *left Y* axis; *black line* calculated spectrum, linked *right Y* axis)

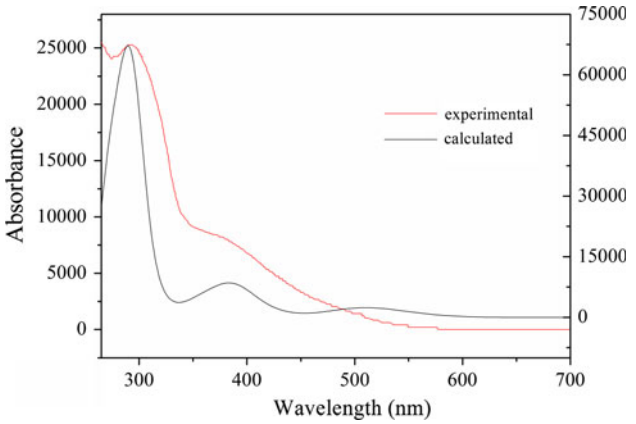

Fig. 6 The experimental and calculated absorption spectra of **3** (*red line* experimental spectrum [20], linked *left Y* axis; *black line* calculated spectrum, linked *right Y* axis)

similar to that of **1** but with some difference in the oscillator strength.

Analogously, compared with **3**, when the COOH groups are also attached to bpy moiety in **4**, the electron excitation for the lowest-lying absorption is changed and contributed by $\{[\pi(\text{TTF})] \rightarrow [\pi^*(\text{bpy}) + \pi^*(\text{TTF})]\}$ and $\{\pi(\text{TTF}) \rightarrow \pi^*(\text{TTF})\}$ for **4** and **3**, respectively. In addition, the absorptions in **4** have an obvious red shift. To summarize, the transitions in the four complexes end in the orbital mastered by the ligand which is appended by the COOH groups. Especially, upon the COOH groups are anchored to both bpy and d*t* (or TTF) ligand in **2** (or **4**), the complexes display lower energy absorption bands with mixed transition character in the UV–visible region, namely the light harvesting capability of the complex can be improved. These absorptions are helpful for charge transfer in DSSC.

3.4 The theoretical understanding in DSSC of 1–4

In our simulation, the DSSC cell is structured as the typical cell described elsewhere [50], in which the semiconductor is TiO_2 with valance band (vb) and conductive band (cb) of 2.5 and −0.7 V (vs. SCE), respectively. The efficiency of the DSSC, that is, the incident photon to current efficiency (IPCE), is a function of the light harvesting efficiency (LHE), the efficient charge injection from the electronic excited state of dye into the conduction band of TiO_2 (Φ_{inj}), and the charge collection efficiency (η_c). The IPCE can be expressed as [49]:

Table 3 Calculated Gibbs free energy (ΔG_{aq}, in au) and redox potential (E^0, versus SCE, in V) of **1**–**4**, together with the available experimental redox potential (E^0_{exp}, vs. SCE, in V) of **1**

Complex	ΔG_{aq}	E^0	E^0_{exp}
1	0.2106	1.540	0.98
2	0.2120	1.579	
3	0.1769	0.623	
4	0.1822	0.768	

[a] The experimental absorption data are from Ref. [20]

$$\mathrm{IPCE} = \mathrm{LHE} \times \Phi_{\mathrm{inj}} \times \eta_c \quad (6)$$

Here, Φ_{inj} depends on the thermodynamic driving force (D) of the vertical excitation:

$$\Phi_{\mathrm{inj}} \propto f(D) \quad (7)$$

$$D = |E^0 - \Delta E - E_{cb}| \quad (8)$$

where E_{cb} is the conductive band of TiO_2 (*vs*. SCE); ΔE is the vertical excitation energy, obtained from TD-DFT calculation. In principle, to make the electronic transfer energetically favorable, the energetics of the excited states of the dye should be high enough to provide a thermodynamic driving force (D) for charge injection.

Calculated Gibbs free energy and redox potential of **1**–**4** together with the available experimental redox potential of **1** are given in Table 3. The general agreement of our results with available experimental data indicates that the approach of this work is rational. The calculated redox potential (see Table 3) of **1** in ground state is 2.3 V bellow the conduction band of TiO_2. Thus, the molecule should absorb energy not less than 2.3 V to excite an electron and than transfer the electron to the conduction band of TiO_2. For **3**, we thus take 1.4 V (vs. SCE) as roughly the least energy a molecule must harvest to inject an electron into the semiconductor. It can be found that all the calculated absorptions of **1** and **3**, except the lowest energy ones, can provide adequate energy to make a valid injection. The lowest-lying absorptions with weaker oscillator strength (less than 0.1) will reduce the LHE and IPCE. Thus, the sensitization of **1** and **3** to solar cell is limited, and this is in accord with the experimental results. Here, we make the approximation that the energetics of the sensitizer are not too different whether it is in methanol solution or bond to TiO_2 film [51].

However, when the COOH groups are attached to both bpy and d*t* in **2**, the absorptions have an obvious red shift compared with **1** and all the excitations have the stronger oscillator strength and large driving force to inject electron (D, from the lowest 0.48 V to the strongest 2.34 V, see Table 3). In **4**, the efficient absorption bands are located at $\lambda < 425$ nm, which can absorb more light than **3**. All of the virtual orbitals in the desired excitations are predominately π^*(bpy) and π^*(d*t*) in **2** (π^*(bpy) and π^*(TTF) in **4**) attached by COOH group, which should facilitate the injection since the sensitizer is anchored to TiO_2 via the COOH ligand. Therefore, after the COOH groups are anchored to both bpy and d*t* (or TTF) ligand in **2** (or **4**), the restructured complexes are more suitable for serving as dyes in solar cell, and the efficiency of the cell sensitized by **2** and **4** should be improved as compared to that by **1** and **3**.

4 Conclusions

Theoretical calculations have been formed on the four Re(I) complexes to reveal the electronic structures, optical properties, focusing on the theoretical understanding and prediction of their performance as sensitizers in DSSC. The calculation results indicate that the FMOs are influenced by the number and position of COOH group. Particularly, the LUMOs are mainly mastered by the ligands attached by the COOH groups, and the COOH groups attached to bpy moiety in **2** and **4** can decrease the energy levels of the LUMO more significantly than those of the HOMO, resulting in narrower HOMO–LUMO energy gaps. Therefore, the absorptions of **2** and **4** have an obvious red shift compared with **1** and **3**. In addition, the electron transition can take place involving this ligand appended by the COOH not only in the MLCT but also in the ILCT transition. On the other hand, the newly designed complex **2** (or **4**) with the bpy and d*t* (or TTF) moieties attached by COOH group has more effective excited state than the parent molecule **1** (or **3**) and may play a better role in DSSC. These results should be helpful for designing new sensitizers in DSSC.

5 Supplementary materials

The partial frontier molecular orbital compositions and energy levels of **1**–**4** are listed in Tables S1–S4. The thermodynamic cycle is shown in Fig. S1.

Acknowledgments The authors are grateful to the financial aid from the National Nature Science Foundation of China (21031003) and Shanxi Natural Science Foundation (2010011012-2).

References

1. Hagfeldt A, Grätzel M (2000) Acc Chem Res 33:269–277
2. Grätzel M (2001) Nature 414:338–344
3. Philippopoulos AI, Terzis A, Raptopoulou CP, Catalano VJ, Falaras P (2007) Eur J Inorg Chem 2007:5633–5644

4. Green MA, Emery K, Hishikawa Y, Warta W (2009) Progr Photovolt Res Appl 17:85–94
5. Yella A, Lee HW, Tsao HN, Yi CY, Chandiran AK, Nazeeruddin MK, Diau EWG, Yeh CY, Zakeeruddin SM, Grätzel M (2011) Science 334:629–634
6. Listorti A, O'Regan B, Durrant JR (2011) Chem Mater 23:3381–3399
7. O'Regan B, Xiaoe L, Ghaddar T (2012) Energy Environ Sci 5:7203–7215
8. Pastore M, Mdoardo E, De Angelis F (2012) J Phy Chem C 116:5965–5973
9. Argazzi R, Iha NYM, Zabri H, Odobel F, Bignozzi CA (2004) Coord Chem Rev 248:1299–1316
10. Chen C-Y, Wu S-J, Chen C-G, Ho K-C (2006) Angew Chem Int Ed 45:5822–5825
11. Kukrek A, Wang D, Hou Y, Zong R, Thummel R (2006) Inorg Chem 45:10131–10137
12. Chen C-Y, Lu H-C, Chen C-G, Ho K-C (2007) Adv Funct Mater 17:29–36
13. Nazeeruddin MK, Péchy P, Renouard T, Zakeeruddin SM, Humphry-Baker R, Comte P, Likda P, Cevey L, Costa E, Shklover V, Spiccia L, Deacon GB, Bignozzi CA, Grätzel M (2001) J Am Chem Soc 123:1613–1624
14. Si Z, Li J, Li B, Zhao F, Liu S, Li W (2007) Inorg Chem 46:6155–6163
15. Wang K, Huang L, Gao L, Jin L, Huang C (2002) Inorg Chem 41:3353–3358
16. Kilsa K, Mayo EI, Brunschwig BS, Gray HB, Lewis NS, Winkler JR (2004) J Phys Chem B 108:15640–15651
17. Sun S–S, Lees AJ (2001) Organometallics 20:2353–2358
18. Hasselmann GM, Meyer GJ (1999) Phys Chem 212:39–44
19. Hasselmann GM, Meyer GJ (1999) J Phys Chem B 103:7671–7675
20. Chen Y, Liu W, Jin J-S, Liu B, Zou Z-G, Zuo J-L, You X-Z (2009) J Organomet Chem 694:763–770
21. Ouahab L, Enoki T (2004) Eur J Inorg Chem 2004:933–941
22. Segura JL, Martin N (2001) Angew Chem Int Ed 40:1372–1409
23. Enoki T, Miyazaki A (2004) Chem Rev 104:5449–5478
24. Ji Y, Zhang R, Li Y-J, Li Y-Z, Zuo J-L, You X-Z (2007) Inorg Chem 46:866–873
25. O'Regan BC, Walley K, Juozapavicius M, Anderson A, Matar F, Ghaddar T, Zakeeruddin SM, Klein C, Durrant JR (2009) J Am Chem Soc 131:3541–3548
26. O'Regan BC, Durrant JR (2009) Acc Chem Res 42:1799–1808
27. Barnes PRF, Liu L, Li X, Anderson AY, Kisserwan H, Ghaddar TH, Durrant JR, O'Regan BC (2009) Nano Letter 9:3532–3538
28. De Angelis F (2010) Chem Phys Lett 493:323–327
29. De Angelis F, Fantacci S, Selloni A, Nazeeruddin MK, Grätzel M (2010) J Phys Chem C 114:6054–6061
30. De Angelis F, Fantacci S, Gebauer R (2011) J Phys Chem Lett 2:813–817
31. De Angelis F, Fantacci S, Selloni A (2008) Nanotechnology 19:424002
32. Frisch MJ, Trucks GW, Schlegel HB, Scuseria GE, Robb MA, Cheeseman JR, Montgomery JA Jr, Vreven T, Kudin KN, Burant JC, Millam JM, Iyengar SS, Tomasi J, Barone V, Mennucci B, Cossi M, Scalmani G, Rega N, Petersson GA, Nakatsuji H, Hada M, Ehara M, Toyota K, Fukuda R, Hasegawa J, Ishida M, Nakajima T, Honda Y, Kitao O, Nakai H, Klene M, Li X, Knox JE, Hratchian HP, Cross JB, Adamo C, Jaramillo J, Gomperts R, Stratmann RE, Yazyev O, Austin AJ, Cammi R, Pomelli C, Ochterski JW, Ayala PY, Morokuma K, Voth GA, Salvador P, Dannenberg JJ, Zakrzewski VG, Dapprich S, Daniels AD, Strain MC, Farkas O, Malick KA, Rabuck D, Raghavachari K, Foresman JB, Ortiz JV, Cui Q, Baboul AG, Clifford S, Cioslowski J, Stefanov BB, Liu G, Liashenko A, Piskorz P, Komaromi I, Martin RL, Fox DJ, Keith T, Al-Laham MA, Peng CY, Nanayakkara A, Hallacombe M, Gill PMW, Johnson B, Wong MW, Chen W, Gonzalez C, Pople JA (2004) Gaussian 03, revision C. 02. Gaussian, Inc., Wallingford
33. Perdew JP, Burke K, Ernzerhof M (1996) Phys Rev Lett 77:3865–3868
34. Adamo C, Barone V (1999) J Chem Phys 110:6158–6170
35. Hay PJ, Wadt WR (1985) J Chem Phys 82:299–310
36. Hay PJ, Wadt WR (1985) J Chem Phys 82:270–283
37. Stratmann RE, Scuseria GE (1998) J Chem Phys 109:8218–8224
38. Matsuzawa NN, Ishitani A (2001) J Phys Chem A 105:4953–4962
39. Casida ME, Jamorski C, Casida KC, Salahub DR (1998) J Chem Phys 108:4439–4449
40. Cossi M, Scalmani G, Regar N, Barone V (2002) J Chem Phys 117:43–54
41. Barone V, Cossi M (1997) J Chem Phys 107:3210–3221
42. Kirgan RA, Rillema DP (2007) J Phys Chem A 111:13157–13162
43. Fantacci S, Angelis FD, Selloni A (2003) J Am Chem Soc 125:4381–4387
44. Censo DD, Fantacci S, Angelis FD, Klein C, Evans N, Kalyanasundaram K, Bolink HJ, Grätzel M, Nazeeruddin MK (2008) Inorg Chem 47:980–989
45. Barolo C, Nazeeruddin MK, Fantacci S, Censo DD, Comte P, Liska P, Viscardi G, Quagliotto P, Angelis FD, Grätzel M (2006) Inorg Chem 45:4642–4653
46. Jaque P, Marenich AV, Cramer CJ, Truhlar DG (2007) J Phys Chem C 111:5783–5799
47. Xu L-C, Shi S, Li J, Liao S-Y, Zheng K-C, Ji L-N (2008) Dalton Trans 2:291–301
48. Busby M, Liard DJ, Motevalli M, Toms H, Vlček A Jr (2004) Inorg Chim Acta 357:167–176
49. Wang J, Bai F-Q, Xia B-H, Feng L, Zhang H-X, Pan Q-J (2011) Phys Chem Phys 13:2206–2213
50. Kalyanasundaram K, Grätzel M (1998) Coord Chem Rev 177:347–414
51. Kuciauskas D, Monat JE, Villahermosa R, Gray HB, Lewis NS, McCusker JK (2002) J Phys Chem B 106:9347–9358